

# A Statistical Dynamical Model to Predict Extreme Events and Anomalous Features in Shallow Water Waves with Abrupt Depth Change

Andrew J. Majda<sup>a,1</sup>, M. N. J. Moore<sup>b</sup>, and Di Qi<sup>a,1</sup>

<sup>a</sup>Department of Mathematics and Center for Atmosphere and Ocean Science, Courant Institute of Mathematical Sciences, New York University, New York, NY 10012;

<sup>b</sup>Department of Mathematics and Geophysical Fluid Dynamics Institute, Florida State University, Tallahassee, FL

This manuscript was compiled on November 27, 2018

**Understanding and predicting extreme events and their anomalous statistics in complex nonlinear systems is a grand challenge in climate, material, and neuroscience, as well as for engineering design. Recent controlled laboratory experiments in weakly turbulent shallow water with abrupt depth change (ADC) exhibit a remarkable transition from nearly Gaussian statistics in incoming wave trains before the ADC to outgoing waves trains after the ADC with extreme anomalous statistics with large positive skewness of the surface height. Here we develop a statistical dynamical model to explain and quantitatively predict the above anomalous statistical behavior as experimental control parameters are varied. The first step is to use incoming and outgoing truncated Korteweg-de Vries (TKdV) equations matched in time at the ADC. The TKdV equation is a Hamiltonian system which induces incoming and outgoing statistical Gibbs invariant measures. The statistical matching of the known nearly Gaussian incoming Gibbs state at the ADC completely determines the predicted anomalous outgoing Gibbs state, which can be calculated by a simple sampling algorithm, verified by direct numerical simulations, and successfully captures key features of the experiment. There is even an analytic formula for the anomalous outgoing skewness. The strategy here should be useful for predicting extreme anomalous statistical behavior in other dispersive media in different settings (21, 22).**

extreme anomalous event | statistical TKdV model | matching Gibbs measures | surface wave displacement and slope

**U**nderstanding and predicting extreme events and their anomalous statistics in complex nonlinear systems is a grand challenge in climate, material and neuroscience as well as for engineering design. This is a very active contemporary topic in applied mathematics with qualitative and quantitative models (1–7) and novel numerical algorithms which overcome the curse of dimensionality for extreme event prediction in large complex systems (2, 8–11). The occurrence of Rogue waves as extreme events within different physical settings of deep water (12–16) and shallow water (17–19) is an important practical topic.

Recent laboratory experiments in weakly turbulent shallow water reveal a remarkable transition from Gaussian to anomalous behavior as surface waves cross an abrupt depth change (ADC). A normally-distributed incoming wave train, upstream of the ADC, transitions to a highly non-Gaussian outgoing wave train, downstream of the ADC, that exhibits large positive skewness of the surface height and more frequent extreme events (20). Here we develop a statistical dynamical model to explain and quantitatively predict this anomalous behavior as experimental control parameters are varied. The first step is to use incoming and outgoing truncated Korteweg-de Vries (TKdV) equations matched in time at the ADC. The TKdV

equation is a Hamiltonian system which induces incoming and outgoing Gibbs invariant measures. The statistical matching of the known nearly Gaussian incoming Gibbs state at the ADC completely determines the predicted anomalous outgoing Gibbs state, which can be calculated by a simple MCMC algorithm, verified by direct numerical simulations, and successfully captures key features of the experiment. There is even an analytic formula for the anomalous outgoing skewness. The strategy here should be useful for predicting extreme anomalous statistical behavior in other dispersive media in different settings (21, 22).

## 1. Experiments showing anomalous wave statistics induced by an abrupt depth change

Controlled laboratory experiments were carried out in (20) to examine the statistical behavior of surface waves crossing an ADC. In these experiments, nearly unidirectional waves are generated by a paddle wheel and propagate through a long, narrow wave tank. Midway through, the waves encounter a step in the bottom topography, and thus abruptly transition to a shallower depth. The paddle wheel is forced with a pseudo-random signal intended to mimic a Gaussian random sea upstream of the ADC. In particular, the paddle angle is

### Significance Statement

**Understanding and predicting extreme events and their anomalous statistics in complex nonlinear systems is a grand challenge in applied sciences as well as for engineering design. Recent controlled laboratory experiments in weakly turbulent shallow water with abrupt depth change exhibit a remarkable transition from nearly Gaussian statistics to extreme anomalous statistics with large positive skewness of the surface height. We develop a statistical dynamical model to explain and quantitatively predict the anomalous statistical behavior. The incoming and outgoing waves are modeled by the truncated Korteweg-de Vries equations statistically matched at the depth change. The statistical matching of the known nearly Gaussian incoming Gibbs state completely determines the predicted anomalous outgoing Gibbs state, and successfully captures key features of the experiment.**

A.J.M. designed the research. A.J.M., M.N.J.M., and D.Q. performed the research. A.J.M., M.N.J.M., and D.Q. wrote the paper.

The authors declare no conflict of interest.

<sup>1</sup>To whom correspondence should be addressed. E-mail: qidi@cims.nyu.edu, jonjon@cims.nyu.edu

125 specified as

$$126 \quad \theta(t) = \theta_0 + \Delta\theta \sum_{n=1}^N a_n \cos(\omega_n t + \delta_n), \quad E \sim (\Delta\theta)^2 \sum_n a_n^2 \omega_n^2.$$

129 where the weights  $a_n$  are Gaussian in spectral space with  
 130 peak frequency  $\omega_p$  and the phases  $\delta_n$  are uniformly distributed  
 131 random variables. The peak frequency gives rise to a char-  
 132 acteristic wavelength  $\lambda_c$  which can be estimated from the  
 133 dispersion relation. The energy  $E$  injected into the system  
 134 is determined by the angle amplitude  $\Delta\theta$ , which is the main  
 135 control parameter varied in (20). Optical measurements of the  
 136 free surface reveal a number of surprising statistical features:

- 138 • Distinct statistics are found between the incoming and  
 139 outgoing wave disturbances: incoming waves display near-  
 140 Gaussian statistics, while outgoing waves skew strongly  
 141 towards positive displacement.
- 142 • The degree of non-Gaussianity present in the outgoing  
 143 waves depends on the injected energy  $E$ : larger energies  
 144 generate stronger skewness in the surface displacement  
 145 PDFs and more extreme events.
- 146 • Compared to the incoming wave train, the power spectrum  
 147 of the outgoing wave field decays more slowly, which  
 148 indicates that the anomalous behavior is associated with  
 149 an elevated level of high frequencies.

## 152 2. Surface wave turbulence modeled by truncated KdV 153 equation with depth dependence

155 The Korteweg-de Vries (KdV) equation is a one-dimensional,  
 156 deterministic model capable of describing (weak?) surface  
 157 wave turbulence. More specifically, KdV is leading-order  
 158 approximation for surface waves governed by a balance of  
 159 nonlinear and dispersive effects, valid in an appropriate far-  
 160 field limit (23). Moreover, KdV has been adapted to describe  
 161 waves propagating over variable depth (23). Here, we consider  
 162 the variable-depth KdV equation truncated at wavenumber  
 163  $\Lambda$  (with  $J = 2\Lambda + 1$  grid points) in order to generate weakly  
 164 turbulent dynamics. The surface displacement is described  
 165 by the state variable  $u_\Lambda^\pm(x, t)$  with superscript ‘-’ for the  
 166 incoming waves and ‘+’ for the outgoing waves. The Galerkin  
 167 truncated variable  $u_\Lambda = \sum_{1 \leq |k| \leq \Lambda} \hat{u}_k(t) e^{ikx}$  is normalized  
 168 with zero mean  $\hat{u}_0 = 0$  and unit energy  $2\pi \sum_{k=1}^\Lambda |\hat{u}_k|^2 = 1$ ,  
 169 which are conserved quantities. Here,  $u_\Lambda \equiv \mathcal{P}_\Lambda u$  denotes the  
 170 subspace projection. The evolution of  $u_\Lambda^\pm$  is governed by the  
 171 truncated KdV equation with depth change  $D_\pm$

$$172 \quad \frac{\partial u_\Lambda^\pm}{\partial t} + \frac{D_\pm^{-3/2}}{2} E_0^{1/2} L_0^{-3/2} \frac{\partial}{\partial x} \mathcal{P}_\Lambda (u_\Lambda^\pm)^2 + D_\pm^{1/2} L_0^{-3} \frac{\partial^3 u_\Lambda^\pm}{\partial x^3} = 0. \quad [1]$$

175 Equation [1] is non-dimensionalized on the periodic domain  $x \in$   
 176  $[-\pi, \pi]$ . The depth is assumed to be unit  $D_- = 1$  before the  
 177 ADC and  $D_+ < 1$  after the ADC. The conserved Hamiltonian  
 178 can be decomposed as

$$180 \quad \mathcal{H}_\Lambda^\pm = D_\pm^{-3/2} E_0^{1/2} L_0^{-3/2} H_3(u_\Lambda^\pm) - D_\pm^{1/2} L_0^{-3} H_2(u_\Lambda^\pm),$$

$$181 \quad H_3(u) = \frac{1}{6} \int_{-\pi}^{\pi} u^3 dx, \quad H_2(u) = \frac{1}{2} \int_{-\pi}^{\pi} \left( \frac{\partial u}{\partial x} \right)^2 dx.$$

184 where we refer to  $H_3$  as the cubic term and  $H_2$  the quadratic  
 185 term. We introduce parameters  $(E_0, L_0, \Lambda)$  based on the fol-  
 186 lowing assumptions:

- 187 • The wavenumber truncation  $\Lambda$  is fixed at a moderate value for generating weakly turbulent dynamics; 188
- 189 • The state variable  $u_\Lambda^\pm$  is normalized with zero mean and unit energy,  $\mathcal{M}(u_\Lambda) = 0, \mathcal{E}(u_\Lambda) = 1$ , which are conserved 190 during evolution. Meanwhile,  $E_0$  characterizes the total 191 energy injected into the system based on the driving 192 amplitude  $\Delta\theta$ ; 193
- 194 • The length scale of the system  $L_0$  is chosen so that the resolved scale  $\Delta x = 2\pi L_0/J$  is comparable to the characteristic wave length  $\lambda_c$  from the experiments. 195

199 Some intuition for how Eq. (1) produces different dynamics 200 on either side of the ADC can be gained by considering the 201 relative contributions of the cubic and quadratic terms to the 202 Hamiltonian  $\mathcal{H}_\Lambda^\pm$ . The depth change,  $D_+ < 1$ , increases the 203 weight of  $H_3$  and decreases that of  $H_2$ , thus promoting the 204 effects of nonlinearity and reducing dispersion. Since  $\frac{\partial u}{\partial x}$  is 205 the slope of the wave height,  $H_2(u)$  measures the wave slope 206 energy.

207 A *deterministic matching condition* is applied to the surface 208 displacement  $u_\Lambda^\pm$  to link the incoming and outgoing wave trains. 209 Assuming the abrupt depth change is met at  $t = T_{\text{ADC}}$ , the 210 matching condition is given by 211

$$212 \quad u_\Lambda^-(x, t)|_{t=T_{\text{ADC}}-} = u_\Lambda^+(x, t)|_{t=T_{\text{ADC}}+},$$

213 Equation [1] is not designed to capture the short scale changes 214 in rapid time. Rather, since we are interested in modeling 215 statistics before and after the ADC, we will examine the long- 216 time dynamics of large-scale structures. 217

### 218 Interpreting experimental parameters in the dynamical model.

219 The model parameters  $(E_0, L_0, \Lambda)$  in [1] can be directly linked 220 to the basic scales from the physical problem. The important 221 characterizing parameters measured from the experiments 222 include:  $\epsilon = \frac{a}{H_0}$  the wave amplitude  $a$  to water depth  $H_0$  223 ratio;  $\delta = \frac{H_0}{\lambda_c}$  the water depth to wavelength scale  $\lambda_c$  ratio; 224 and  $D_0 = \frac{d}{H_0}$  the normalized wave depth ratio with incoming 225 flow depth  $d = H_0$  to the outgoing flow depth  $d < H_0$ . The 226 interpretations and reference values of these model parameters 227 are based on the experimental setup (20). By comparing the 228 characteristic physical scales, the normalized TKdV equation 229 [1] can be linked directly with the measured non-dimensional 230 quantities by 231

$$232 \quad L_0 = 6^{\frac{1}{3}} \left( M \epsilon^{\frac{1}{2}} \delta^{-1} \right), \quad E_0 = \frac{27}{2} \gamma^{-2} \left( M \epsilon^{\frac{1}{2}} \delta^{-1} \right), \quad [2]$$

233 where  $M$  defines the computational domain size  $M\lambda_c$  as  $M$ -  
 234 multiple of the characteristic wavelength  $\lambda_c$ , and  $\gamma = \frac{U}{a}$  rep-  
 235 presents the factor to normalize the total energy in the state  
 236 variable  $u_\Lambda$  to one. 237

238 Consider the spatial discretization  $J = 2\Lambda + 1$  so that the 239 smallest resolved scale is comparable with the characteristic 240 wavelength 241

$$242 \quad \Delta x = \frac{2\pi M \lambda_c}{J} \lesssim \lambda_c \Rightarrow M = \frac{J}{2\pi} \sim 5, \quad J = 32.$$

243 Therefore in the practical numerical simulations, we pick 244  $M = 5$  and  $\gamma$  varies in the range  $[0.5, 1]$ . Using the reference 245 experimental measurements (20),  $\epsilon \in [0.0024, 0.024]$ ,  $\delta \sim 0.22$ , 246 and  $D_0$  changes from 1 to 0.24 before and after the depth 247 248

249 change. The reference values for the model scales can be esti-  
 250 mated in the range  $L_0 \in [2, 6]$  and  $E_0 \in [50, 200]$ . These are  
 251 the values we will test in the direct numerical simulations. See  
 252 details about the derivation from scale analysis in *SI Appendix*,  
 253 A.

254

### 255 3. Equilibrium statistical mechanics for generating the 256 stationary invariant measure

257 Since the TKdV equation satisfies the Liouville property, the  
 258 equilibrium invariant measure can be described by an equi-  
 259 librium statistical formulism (24–26) using a Gibbs measure  
 260 with the conserved energy  $\mathcal{E}_\Lambda$  and Hamiltonian  $\mathcal{H}_\Lambda$ . The equi-  
 261 librium invariant measure is dictated by the conservation laws  
 262 in the TKdV equation. In the case with fixed total energy  $E_0$ ,  
 263 this is the *mixed Gibbs measure* in the truncated model with  
 264 microcanonical energy and canonical Hamiltonian ensembles  
 265 (24)

266 
$$\mathcal{G}_\theta^\pm(u_\Lambda^\pm; E_0) = C_\theta^\pm \exp(-\theta^\pm \mathcal{H}(u_\Lambda^\pm)) \delta(\mathcal{E}(u_\Lambda^\pm) - E_0), \quad [3]$$

267 with  $\theta$  representing the “inverse temperature”. The distinct  
 268 statistics in the upstream and downstream waves can be con-  
 269 trolled by the value of  $\theta$ . Negative temperature,  $\theta^\pm < 0$ , is  
 270 the appropriate regime to predict the experiments as shown  
 271 below. In the incoming flow field, the inverse temperature  $\theta^-$   
 272 is chosen so that  $\mathcal{G}_\theta^-$  has Gaussian statistics. Using the above  
 273 invariant measures [3], the expectation of any functional  $F(u)$   
 274 can be computed based on the Gibbs measure

275 
$$\langle F \rangle_{\mathcal{G}_\theta} \equiv \int F(u) \mathcal{G}_\theta(u) du.$$

276 The value of  $\theta$  in the invariant measure is specified from  $\langle H_\Lambda \rangle_{\mathcal{G}_\theta}$   
 277 (24, 26). The invariant measure also predicts an equilibrium  
 278 energy spectrum without running the TKdV equation directly.  
 279 On the other hand, the time autocorrelation and transient  
 280 statistics about the state variable  $u_\Lambda$  cannot be recovered from  
 281 the statistical theory.

282 **Statistical matching condition in invariant measures before  
 283 and after the abrupt depth change.** The Gibbs measures  $\mathcal{G}_\theta^\pm$   
 284 are defined based on the different inverse temperatures  $\theta^\pm$  on  
 285 the two sides of the solutions

286 
$$\begin{aligned} \mu_t^-(u_\Lambda^-; D_-), \quad u_\Lambda |_{t=T_{ADC}-} &= u_0, \quad t < T_{ADC}; \\ \mu_t^+(u_\Lambda^+; D_+), \quad u_\Lambda |_{t=T_{ADC}+} &= u_0, \quad t > T_{ADC}, \end{aligned}$$

287 where  $u_0$  represents the deterministic matching condition be-  
 288 tween the incoming and outgoing waves. The two distributions,  
 289  $\mu_t^-, \mu_t^+$  should also be matched at the depth change location  
 290  $T_{ADC}$ , so that,

291 
$$\mu_{t=T_{ADC}}^-(u_\Lambda) = \mu_{t=T_{ADC}}^+(u_\Lambda).$$

292 In matching the flow statistics before and after the abrupt  
 293 depth change, we first use the conservation of the determinis-  
 294 tic Hamiltonian  $H_\Lambda^+$  after the depth change. Then assuming  
 295 ergodicity (24, 25), the statistical expectation for the Hamil-  
 296 tonian  $\langle H_\Lambda^+ \rangle$  is conserved in time after the depth change at  
 297  $t = T_{ADC}$  and should stay in the same value as the system ap-  
 298 proaches equilibrium as  $t \rightarrow \infty$ . The final statistical matching  
 299 condition to get the outgoing flow statistics with parameter  
 300  $\theta^+$  can be found by

301 
$$\langle H_\Lambda^+ \rangle_{\mathcal{G}_\theta^+} = \langle H_\Lambda^+ \rangle_{\mathcal{G}_\theta^-}, \quad [4]$$

302 with the outgoing flow Hamiltonian  $H_\Lambda^+$  and the Gibbs mea-  
 303 sures  $\mathcal{G}_\theta^\pm$  before and after the abrupt depth change.

### 304 4. The nearly Gaussian incoming statistical state

305 The incoming flow is always characterized by a near-Gaussian  
 306 distribution in the wave displacement. It is found that a  
 307 physically consistent Gibbs measure should take negative val-  
 308 ues in the inverse temperature parameter  $\theta < 0$ , where a  
 309 proper distribution function and a decaying energy spectrum  
 310 are generated (see (26) and *SI Appendix*, B.1 for the explicit  
 311 simulation results). The upstream Gibbs measure  $\mathcal{G}_\theta^-$  with  
 312  $D_- = 1$  displays a wide parameter regime in  $(\theta^-, E_0)$  with  
 313 near-Gaussian statistics. In the left panel of Figure 1 (a), the  
 314 inflow skewness  $\kappa_3^-$  varies only slightly with changing values of  
 315  $E_0$  and  $\theta^-$ . The incoming flow PDF then can be determined  
 316 by picking the proper parameter value  $\theta^-$  in the near Gaus-  
 317 sian regime with small skewness. In contrast, the downstream  
 318 Gibbs measure  $\mathcal{G}_\theta^+$  with  $D_+ = 0.24$  shown in the right panel  
 319 of Figure 1 (a) generates much larger skewness  $\kappa_3^+$  as the  
 320 absolute value of  $\theta^+$  and the total energy level  $E_0$  increases.  
 321 The solid lines in Figure 1 (c) offer a further confirmation of  
 322 the transition from near-Gaussian statistics with small  $\kappa_3^-$  to  
 323 a strongly skewed distribution  $\kappa_3^+$  after the depth change.

324 In the next step, the value of the downstream  $\theta^+$  is deter-  
 325 mined based on the matching condition [4]. The expectation  
 326  $\langle H_\Lambda^+ \rangle_{\mathcal{G}_\theta^-}$  about the incoming flow Gibbs measure can be cal-  
 327 culated according to the predetermined parameter values of  
 328  $\theta^-$  as well as  $E_0$  from the previous step. For the direct nu-  
 329 matical experiments shown later in Figure 2, we pick proper  
 330 choices of test parameter values as  $L_0 = 6, E_0 = 100$  and  
 331  $\theta^- = -0.1, -0.3, -0.5$ . More test cases with different system  
 332 energy  $E_0$  can be found in *SI Appendix*, B.2 where similar  
 333 transition from near Gaussian symmetric PDFs to skewed  
 334 PDFs in the flow state  $u_\Lambda^\pm$  can always be observed.

335 **Direct numerical model simulations.** Besides the prediction of  
 336 equilibrium statistical measures from the equilibrium statisti-  
 337 cal approach, another way to predict the downstream model  
 338 statistics is through running the dynamical model [1] directly.  
 339 The TKdV equation is found to be ergodic with proper mixing  
 340 property as measured by the decay of autocorrelations as long  
 341 as the system starts from a negative inverse temperature state  
 342 as described before. For direct numerical simulations of the  
 343 TKdV equations, a proper symplectic integrator is required to  
 344 guarantee the Hamiltonian and energy are conserved in time.  
 345 It is crucial to use the symplectic scheme to guarantee the  
 346 exact conservation of the energy and Hamiltonian since they  
 347 are playing the central role in generating the invariant measure  
 348 and the statistical matching. The symplectic schemes used  
 349 here for the time integration of the equation is the 4th-order  
 350 midpoint method (27). Details about the mixing properties  
 351 from different initial states and the numerical algorithm are  
 352 described in *SI Appendix*, C.

### 353 5. Predicting extreme anomalous behavior after the 354 ADC by statistical matching

355 With the inflow statistics well described and the numerical  
 356 scheme set up, we are able to predict the downstream anomalous  
 357 statistics starting from the near-Gaussian incoming flow  
 358 going through the abrupt depth change from  $D_- = 1$  to  
 359  $D_+ = 0.24$ .

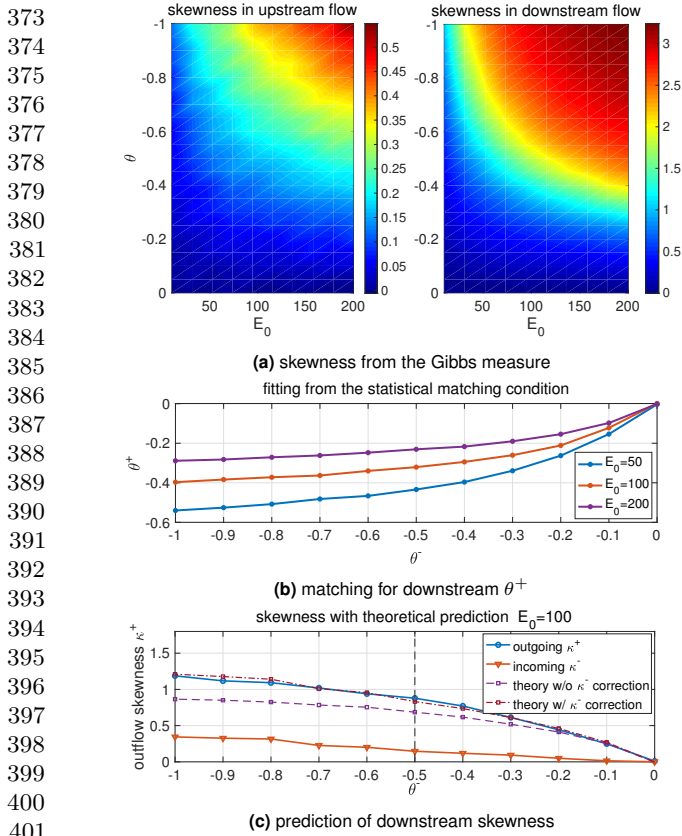


**Fig. 1.** First row: skewness from the Gibbs measures in incoming and outgoing flow states with different values of total energy  $E_0$  and inverse temperature  $\theta$  (notice the different scales in the incoming and outgoing flows); Second row: outgoing flow parameter  $\theta^+$  as a function of the incoming flow  $\theta^-$  computed from the statistical matching condition with three energy level  $E_0$ ; Last row: skewness in the outgoing flow with the matched value of  $\theta^+$  as a function of the inflow parameter  $\theta^-$  (the theoretical predictions using [5] are compared).

$D_+ = 0.24$ . First, we consider the statistical prediction in the downstream equilibrium measure directly from the matching condition. The downstream parameter value  $\theta^+$  is determined by solving the nonlinear equation [4] as a function of  $\theta^+$ ,  $F(\theta^+) = \langle H_\Lambda^+ \rangle_{\mathcal{G}_\theta^+}(\theta^+) - \langle H_\Lambda^+ \rangle_{\mathcal{G}_\theta^-} = 0$ . In the numerical approach, we adopt a modified secant method avoiding the stiffness in the parameter regime (see the *SI Appendix, B.2* for the algorithm). The fitted solution is plotted in Figure 1 (b) as a function of the proposed inflow  $\theta^-$ . A nonlinear  $\theta^-$ - $\theta^+$  relation is discovered from the matching condition. The downstream inverse temperature  $\theta^+$  will finally saturate at some level. The corresponding downstream skewness of the wave displacement  $u_\Lambda$  predicted from the statistical matching of Gibbs measures is plotted in Figure 1 (c). In general, a large positive skewness for outgoing flow  $\kappa_3^+$  is predicted from the theory, while the incoming flow skewness  $\kappa_3^-$  is kept in a small value in a wide range of  $\theta^-$ . Note that with  $\theta^- \sim 0$  (that is, using the microcanonical ensemble only with energy conservation), the outflow statistics are also near Gaussian with weak skewness. The skewness in the outflow statistics grows as the inflow parameter value  $\theta^-$  increases in amplitude.

For a second approach, we can use direct numerical simulations starting from the initial state sampled from the incoming flow Gibbs measure  $\mathcal{G}_\theta^-$  and check the transient changes in the

model statistics. Figure 2 illustrates the change of statistics as the flow goes through the abrupt depth change. The first row plots the changes in the skewness and kurtosis for the state variable  $u_\Lambda$  after the depth change at  $t = 0$ . The PDFs in the incoming and outgoing flow states are compared with three different initial inverse temperatures  $\theta^-$ . After the depth changes to  $D_0 = 0.24$  abruptly at  $t = 0$ , both the skewness and kurtosis jump to a much larger value in a short time, implying the rapid transition to a highly skewed non-Gaussian statistical regime after the depth change. Further from Figure 2, different initial skewness (but all relatively small) is set due to the various values of  $\theta^-$ . With small  $\theta^- = -0.1$ , the change in the skewness is not very obvious (see the second row of Figure 2 for the incoming and outgoing PDFs of  $u_\Lambda$ ). In comparison, if the incoming flow starts from the initial parameter  $\theta^- = -0.3$  and  $\theta^- = -0.5$ , much larger increase in the skewness is induced from the abrupt depth change. Furthermore, in the detailed plots in the third row of Figure 2 for the downstream PDFs under logarithmic scale, fat tails towards the positive direction can be observed, which represent the extreme events in the downstream flow (see also Figure 3 for the time-series of  $u_\Lambda$ ).

As a result, the downstream statistics in final equilibrium predicted from the direct numerical simulations here agree with the equilibrium statistical mechanics prediction illustrated in Figure 1. The prediction from these two different approaches confirm each other.

## 6. Analytic formula for the upstream skewness after the ADC

A statistical link between the upstream and downstream energy spectra can be found for an analytical prediction of the skewness in the flow state  $u$  after the ADC. The skewness of the state variable  $u_j$  at one spatial grid point is defined as the ratio between the third and second moments

$$\kappa_3 = \langle u_j^3 \rangle_\mu / \langle u_j^2 \rangle_\mu^{3/2}.$$

Now we introduce mild assumptions on the distribution functions:

- The upstream equilibrium measure  $\mu_-$  has a relatively small skewness so that

$$\langle H_3 \rangle_{\mu_-} = \frac{1}{6} \int_{-\pi}^{\pi} \langle u^3 \rangle_{\mu_-} dx \equiv \epsilon;$$

- The downstream equilibrium measure  $\mu_+$  is homogeneous at each physical grid point, so that the second and third moments are invariant at each grid point

$$\langle u_j^2 \rangle_{\mu_+} = \sigma^2 = \pi^{-1}, \quad \langle u_j^3 \rangle_{\mu_+} = \sigma^3 \kappa_3 = \pi^{-3/2} \kappa_3^+.$$

Then the skewness of the downstream state variable  $u_\Lambda^+$  after the ADC is given by the difference between the inflow and outflow wave slope energy of  $u_x$

$$\kappa_3^+ = \frac{3}{2} \pi^{1/2} L_0^{-3/2} E_0^{-1/2} D_+^2 \int_{-\pi}^{\pi} [\langle u_x^2 \rangle_{\mu_+} - \langle u_x^2 \rangle_{\mu_-}] dx + 3\pi^{1/2} \epsilon.$$

The detailed derivation is shown in *SI Appendix, B.2*. In particular, the downstream skewness with near-Gaussian inflow

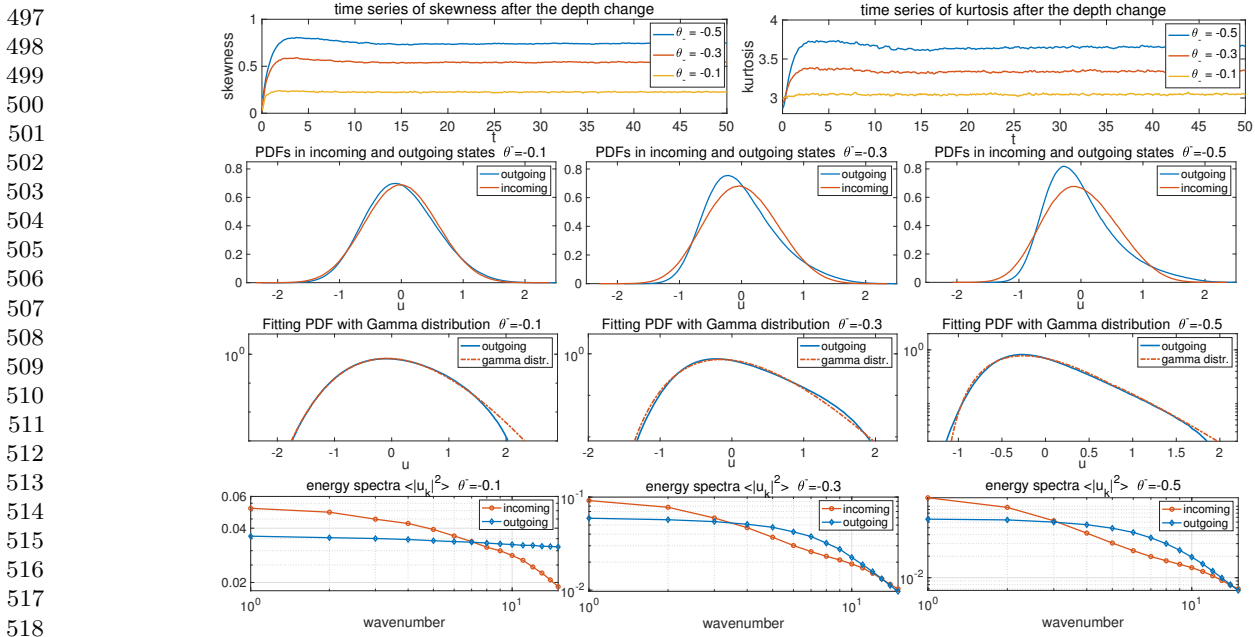


Fig. 2. Changes in the statistics of the flow state going through the abrupt depth change. The initial ensemble is set with the incoming flow Gibbs measure with different inverse temperature  $\theta^-$ . First row: time evolution of the skewness and kurtosis. The abrupt depth change is taking place at  $t = 0$ ; Second row: inflow and outflow PDFs of  $u_\Lambda$ ; Third row: the downstream PDFs fitted with Gamma distributions with consistent variance and skewness (in log coordinate in  $y$ ); Last row: energy spectra in the incoming and outgoing flows.

statistics  $\epsilon \ll 1$  is positive if and only if the difference of the incoming and outgoing wave slope energy is positive. This means that there is more small scale wave slope energy in the outgoing state. As an evidence, in the last row of Figure 2 in all the weak and strong skewness cases, the outflow energy spectrum always has a slower decay rate than the inflow energy spectrum which possesses stronger energy in larger scales and weaker energy in the smaller scales.

In Figure 1 (c), we compare the accuracy of the theoretical estimation [5] with numerical tests. In the regime with small incoming inverse temperature  $\theta^-$ , the theoretical formula offers a quite accurate approximation of the third-order skewness using only information from the second-order moments of the wave-slope spectrum.

## 7. Key features from experiments captured by the statistical dynamical model

In this final section, we emphasize the crucial features generated by the statistical dynamical model [1] by making comparison with the experimental observations in (20). As from the scale analysis displayed in Section 2, the theory is set in the same parameter regime as the experimental setup.

- The transition from near-Gaussian to skewed non-Gaussian distribution as well as the jump in both skewness and kurtosis observed in the experiment observations (Fig. 1 of (20)) can be characterized by the statistical model simulation results (see the first and second row of Figure 2). Notice that the difference in the decay of third and fourth moments in the far end of the downstream regime from the experimental data is due to the dissipation effect in the flow from the wave absorbers that is not modeled in the statistical model here. The model simulation time-series plotted in Figure 3 can be compared with

the observed time sequences from experiments (Fig. 1 of (20)). The downstream simulation generates waves with strong and frequent intermittency towards the positive displacement, while the upstream waves show symmetric displacements in two directions with at most small peaks in slow time. Even in the time-series at a single location  $x = 0$ , the long-time variation displays similar structures.

- The downstream PDFs in experimental data are estimated with a Gamma distribution in Fig. 2 of (20). Here in the same way, we can fit the highly skewed outgoing flow PDFs from the numerical results with the Gamma distribution

$$\rho(u; k, \alpha) = \frac{e^{-k} \alpha^{-1}}{\Gamma(k)} (k + \alpha^{-1} u)^{k-1} e^{-\alpha^{-1} u}.$$

The parameters  $(k, \alpha)$  in the Gamma distribution are fitted according to the measured statistics in skewness and variance, that is,  $\sigma^2 = k\alpha^2$ ,  $\kappa_3 = 2/\sqrt{k}$ . And the excess kurtosis of the Gamma distribution can be recovered as  $\kappa_4 = 6/k$ . As shown in the third row of Figure 2, excellent agreement in the PDFs with the Gamma distributions is reached in consistency with the experimental data observations. The accuracy with this approximation increases as the initial inverse temperature  $\theta^-$  increases in value to generate more skewed distribution functions.

- The experiments also have the up and down stream power spectra in time (Fig. 4 of (20)), which shows more energy at small time scales, i.e., a relatively slower decay rate in the downstream compared with the upstream case. This is also observed in the direct numerical simulations here (detailed results shown in SI Appendix, C.2). The downstream state contains more energetic high frequencies. The peak frequency illustrates the characteristic

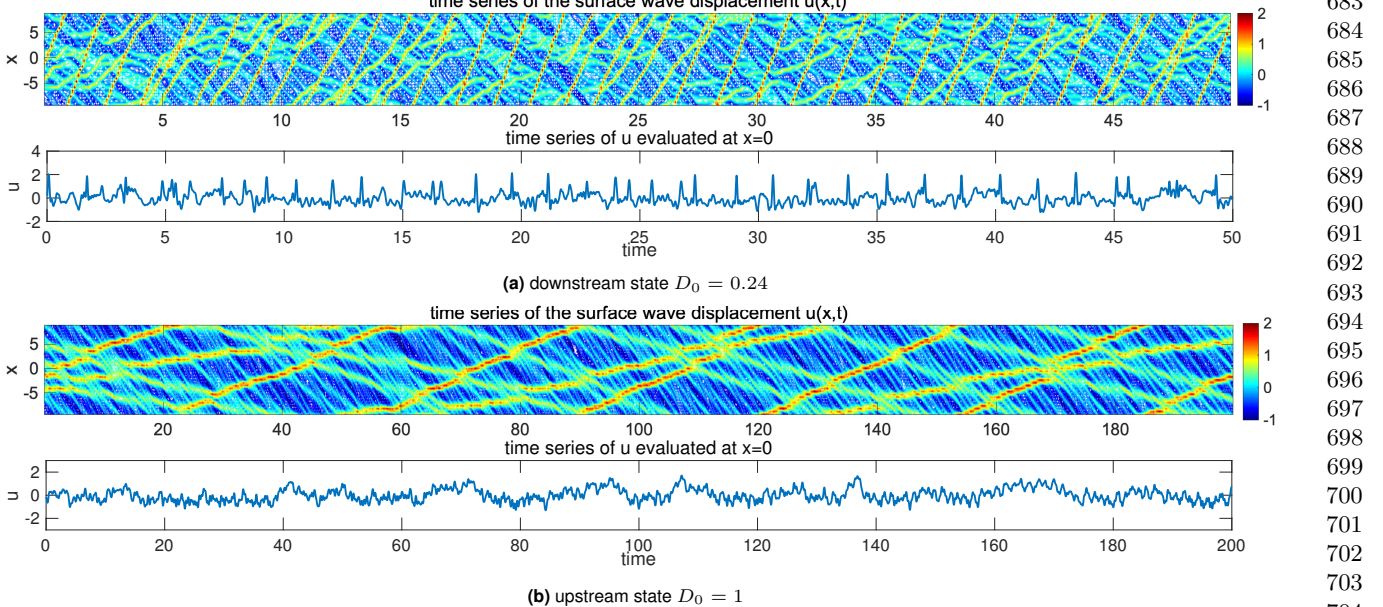


Fig. 3. Realization of the downstream and upstream flow solutions  $u_A^\pm$ . Note the larger vertical scale in the downstream time-series plot.

time scale of the transporting wave trains along the water tank.

I do not understand the last sentence above. Why does the peak frequency illustrate the occurrence of transporting water waves?

## 8. Concluding discussion

We have developed a statistical dynamical model to explain and predict extreme events and anomalous features of shallow water waves crossing an abrupt depth change. The theory is based on the dynamical modeling strategy consisting of the TKdV equation matched at the abrupt depth change with conservation of energy and Hamiltonian. Predictions can be made of the extreme events and anomalous features by matching

incoming and outgoing statistical Gibbs measures before and after the abrupt depth transition. The statistical matching of the known nearly Gaussian incoming Gibbs state completely determines the predicted anomalous outgoing Gibbs state, which can be calculated by a simple sampling algorithm, verified by direct numerical simulations, and successfully captures key features of the experiment. An analytic formula for the anomalous outgoing skewness is also derived. The strategy here should be useful for predicting extreme statistical events in other dispersive media in different settings.

**ACKNOWLEDGMENTS.** This research of A. J. M. is partially supported by the Office of Naval Research through MURI N00014-16-1-2161. D. Q. is supported as a postdoctoral fellow on the second grant. M.N.J.M would like to acknowledge support from Simons grant 524259.

1. Majda AJ, Branicki M (2012) Lessons in uncertainty quantification for turbulent dynamical systems. *Discrete & Continuous Dynamical Systems-A* 32(9):3133–3221.
2. Mohamad MA, Sapsis TP (2018) A sequential sampling strategy for extreme event statistics in nonlinear dynamical systems. *Proceedings of the National Academy of Sciences* 115(44):11138–11143.
3. Qi D, Majda AJ (2016) Predicting fat-tailed intermittent probability distributions in passive scalar turbulence with imperfect models through empirical information theory. *Communications in Mathematical Sciences* 14(6):1687–1722.
4. Majda AJ, Tong XT (2015) Intermittency in turbulent diffusion models with a mean gradient. *Nonlinearity* 28(11):4171–4208.
5. Majda AJ, Chen N (2018) Model error, information barriers, state estimation and prediction in complex multiscale systems. *Entropy* 20(9):644.
6. Majda AJ, Tong XT (2018) Simple nonlinear models with rigorous extreme events and heavy tails. *arXiv preprint arXiv:1805.05615*.
7. Thual S, Majda AJ, Chen N, Stechmann SN (2016) Simple stochastic model for el nino with westerly wind bursts. *Proceedings of the National Academy of Sciences* 113(37):10245–10250.
8. Chen N, Majda AJ (2018) Efficient statistically accurate algorithms for the Fokker–Planck equation in large dimensions. *Journal of Computational Physics* 354:242–268.
9. Chen N, Majda AJ (2017) Beating the curse of dimension with accurate statistics for the Fokker–Planck equation in complex turbulent systems. *Proceedings of the National Academy of Sciences* 114(49):12864–12869.
10. Chen N, Majda AJ (2018) Conditional Gaussian systems for multiscale nonlinear stochastic systems: Prediction, state estimation and uncertainty quantification. *Entropy* 20(7):509.
11. Qi D, Majda AJ (2018) Predicting extreme events for passive scalar turbulence in two-layer baroclinic flows through reduced-order stochastic models. *Communications in Mathematical Sciences* 16(1):17–51.
12. Adcock TA, Taylor PH (2014) The physics of anomalous ('rogue') ocean waves. *Reports on Progress in Physics* 77(10):105901.
63. | Cite this as: Majda AJ, Chen N, Stechmann SN (2019) Unidirectional deep-water wave groups. *Physical Review E* 91(6):063204.
14. Farazmand M, Sapsis TP (2017) Reduced-order prediction of rogue waves in two-dimensional deep-water waves. *Journal of Computational Physics* 340:418–434.
15. Onorato M, Osborne AR, Serio M, Bertone S (2001) Freak waves in random oceanic sea states. *Physical Review Letters* 86(25):5831–5834.
16. Dematteis G, Grafke T, Vanden-Eijnden E (2018) Rogue waves and large deviations in deep sea. *Proceedings of the National Academy of Sciences* 115(5):855–860.
17. Sergeeva A, Pelinovsky E, Talipova T (2011) Nonlinear random wave field in shallow water: variable Korteweg-de Vries framework. *Natural Hazards and Earth System Sciences* 11(2):323–330.
18. Trulsen K, Zeng H, Gramstad O (2012) Laboratory evidence of freak waves provoked by non-uniform bathymetry. *Physics of Fluids* 24(9):097101.
19. Viotti C, Dias F (2014) Extreme waves induced by strong depth transitions: Fully nonlinear results. *Physics of Fluids* 26(5):051705.
20. Bolles CT, Speer K, Moore MNJ (2018) Anomalous wave statistics induced by abrupt depth change. *arXiv preprint arXiv:1808.07958*.
21. Solli D, Ropers C, Koonath P, Jalali B (2007) Optical rogue waves. *Nature* 450(7172):1054.
22. Höhmann R, Kuhl U, Stöckmann HJ, Kaplan L, Heller E (2010) Freak waves in the linear regime: A microwave study. *Physical review letters* 104(9):093901.
23. Johnson RS (1997) *A modern introduction to the mathematical theory of water waves*. (Cambridge university press) Vol. 19.
24. Abramov RV, Kovačić G, Majda AJ (2003) Hamiltonian structure and statistically relevant conserved quantities for the truncated Burgers-Hopf equation. *Communications on Pure and Applied Mathematics: A Journal Issued by the Courant Institute of Mathematical Sciences* 56(1):1–46.
25. Majda A, Wang X (2006) *Nonlinear dynamics and statistical theories for basic geophysical flows*. (Cambridge University Press).
26. Bajars J, Frank J, Leimkuhler B (2013) Weakly coupled heat bath models for Gibbs-like invariant states in nonlinear wave equations. *Nonlinearity* 26(7):1945–1973.
27. McLachlan R (1993) Symplectic integration of hamiltonian wave equations. *Numerische Mathematik* 66(1):465–492.